AD_____

Award Number: W81XWH-04-1-0411

TITLE: Simultaneous Monitoring of Vascular Oxygenation and Tissue Oxygen Tension of Breast Tumors Under Hyperbaric Oxygen Exposure

PRINCIPAL INVESTIGATOR: Mengna Xia

CONTRACTING ORGANIZATION: The University of Texas at Arlington
Arlington, TX 76019

REPORT DATE: April 2005

TYPE OF REPORT: Annual Summary

PREPARED FOR: U.S. Army Medical Research and Materiel Command
Fort Detrick, Maryland 21702-5012

REPORT DOCUMENTATION PAGE

Form Approved
OMB No. 0704-0188

1. REPORT DATE	2. REPORT TYPE	3. DATES COVERED
01-04-2005	Annual Summary	9 Mar 2004 – 8 Mar 2005

4. TITLE AND SUBTITLE

Simultaneous Monitoring of Vascular Oxygenation and Tissue Oxygen Tension of Breast Tumors Under Hyperbaric Oxygen Exposure

5a. CONTRACT NUMBER

5b. GRANT NUMBER
W81XWH-04-1-0411

5c. PROGRAM ELEMENT NUMBER

6. AUTHOR(S)

Mengna Xia

5d. PROJECT NUMBER

5e. TASK NUMBER

5f. WORK UNIT NUMBER

7. PERFORMING ORGANIZATION NAME(S) AND ADDRESS(ES)

The University of Texas at Arlington
Arlington, TX 76019

8. PERFORMING ORGANIZATION REPORT NUMBER

9. SPONSORING / MONITORING AGENCY NAME(S) AND ADDRESS(ES)
U.S. Army Medical Research and Materiel Command
Fort Detrick, Maryland 21702-5012

10. SPONSOR/MONITOR'S ACRONYM(S)

11. SPONSOR/MONITOR'S REPORT NUMBER(S)

12. DISTRIBUTION / AVAILABILITY STATEMENT
Approved for Public Release; Distribution Unlimited

13. SUPPLEMENTARY NOTES

14. ABSTRACT

The goals of the study in the first stage are 1) to develop a mathematic model by which we can derive tumor blood flow and metabolic rate of oxygen from hemoglobin concentration during interventions, 2) to investigate vascular oxygenation and tissue oxygen tension of breast tumor under continuous normobaric and hyperbaric oxygen exposures with several gas interventions, using near-infrared spectroscopy and FOXY oxygen sensor simultaneously. The results show that the fitted tumor blood flow and metabolic rate of oxygen showed different responses between oxygen and carbogen interventions by applying our model. The simultaneous measurements by broadband diffuse spectroscopy and FOXY oxygen sensor demonstrate that hyperbaric oxygen improves both the tumor vascular and tissue oxygen level more effectively than normobaric oxygen.

15. SUBJECT TERMS
Technology Development, Radiologic Sciences, Tumor Therapy Planning and Prognosis, Tumor Physiology Monitoring

16. SECURITY CLASSIFICATION OF:			17. LIMITATION OF ABSTRACT	18. NUMBER OF PAGES	19a. NAME OF RESPONSIBLE PERSON
a. REPORT	b. ABSTRACT	c. THIS PAGE			USAMRMC
U	U	U	UU	50	19b. TELEPHONE NUMBER *(include area code)*

Table of Contents

2004-2005 ANNUAL PROGRESS REPORT

This report presents the specific aims and accomplishments of our breast cancer research project during the first year of funding sponsored by the US Department of the Army.

Introduction

The goal of this research project is to apply the multiple monitoring techniques, i.e. Near infrared spectroscopy (NIRS), FOXY oxygen sensor and ^{19}F MR EP imaging of Hexafluorobenzene (HFB), to prove the following hypotheses: combination of hyperbaric oxygen (HBO) intervention can significantly improve breast tumor oxygenation, and that tumor oxygenation remains elevated for a substantial period of time even after HBO exposure, which may be a novel approach to enhance radiosensitivity. If our hypotheses are proven to be true, this study will lead to an optimal intervention plan to improve tumor oxygenation and to determine an optimal time interval after HBO decompression for radiotherapy. Such a novel approach will largely enhance the efficiency of non-surgical therapies for breast tumor treatment and provide a novel prognostic tool for clinical practice. This study will also provide a better understanding of tumor vasculature and tissue oxygen dynamics and spatial heterogeneity under HBO exposure.

The project has three specific aims:

Aim 1: to determine the absolute values of oxygenated hemoglobin concentration, [HbO_2], and hemoglobin oxygen saturation, SO_2, in solid breast tumors from the NIRS measurements.

Aim 2: to investigate vascular oxygenation and tissue oxygen tension of breast tumors under continuous normobaric and hyperbaric oxygen exposures with several gas interventions, using both a single-channel NIRS system and 3-channel FOXY pO_2 system simultaneously.

Aim 3: to investigate global and local dynamics of tumor vascular [HbO_2] and tissue pO_2 of breast tumors immediately after HBO exposure by using both three-channel NIRS and ^{19}F MR EP imaging simultaneously.

Body of the report

As mentioned above, the purpose of this project is to investigate vascular and tissue oxygen dynamics in breast tumors by using multiple techniques: NIRS, FOXY and MRI. In the first year, my focus is to develop algorithm to calculate absolute value of hemoglobin concentration (month 1-8), to obtain the appropriate knowledge and skills for conducting the project (month 9-14). I have accomplished not only those two tasks (month 1-14) but also a part of task 3 (month 14-30).

Task 1: to develop a numerical algorithm so as to determine the absolute value of HbO_2 and SO_2 in solid breast tumors from near infrared spectroscopic (NIRS) measurements by using the non-linear, least-squared optimization approach. (months 1-8)

Since ***task 1*** has been accomplished by other members of our group, the PI has switched to another task of equal importance.

New task 1: develop a mathematical model, which relates the blood flow and metabolic rate of oxygen in breast tumors to hemoglobin concentration so that NIRS can be used to estimate changes in tumor blood flow (TBF) and tumor metabolic rate of oxygen ($TMRO_2$) non-invasively during hyperoxic gas interventions in rat tumors. Such a model will shed light on tumor vascular adaptation to therapeutic intervention, giving us a better understanding of physiological responses of tumors to intervention. This task has been accomplished, as reported below:

In order to find the relationship between the hemoglobin concentration and metabolic rate of oxygen during intervention, there is a mathematical equation, called as the ***ratio method*** which states that metabolic rate of oxygen could be derived from blood flow and hemoglobin concentration (Jones *et al* 2001). NIRS measurements have enabled us to quantify relative changes in hemoglobin concentration during inhalation but have not been used to measure blood flow changes. Thus, it is necessary to explore a mathematical model that relates changes in blood flow to changes in blood volume (i.e., total hemoglobin concentration) in order to estimate flow changes based on the NIRS data. Boas et al have utilized the ***Windkessel model*** to fit a flow-volume relationship and estimated the relative changes of cerebral blood flow during brain activation (Boas *et al* 2003), with a relatively good fit to the NIRS experimental data. Following the same strategy, here, oxygen/carbogen induced tumor blood flow changes were estimated by fitting the Windkessel model (Mandeville *et al* 1999) to the measured Δ[HbT], with the modification of physiological meaning of tumor vasculature.

Step 1: The Windkessel model used for estimating blood flow from [HbT]

The Windkessel model relates blood flow to blood volume. With a few assumptions, we can thus estimate the blood flow response to intervention from the measured Δ[HbT] since Δ[HbT] is directly proportional to changes in blood volume. The Windkessel model is based on the conservation of mass to associate changes in blood volume with changes in blood flow through the regional arterial, capillary and venous compartments, with capillaries and veins lumped together and named a Windkessel compartment. The model proposes that the flow into the Windkessel compartment is largely determined by the vasomotor control of arterioles, and that the capillaries and veins passively respond to arterial pressure changes (Mandeville *et al* 1999). Briefly described here, the model has the following definitions and relationships:

1) In analogy to Ohm's law, we have $P(t)=F(t)R(t)$,

where F is the blood flow, P is the blood pressure, and R is the vascular resistance;

2) The Windkessel model assumes $V_w(t)=AP_w(t)^{1/\beta}$,

where V_w and P_w are the volume and pressure of the Windkessel compartment, respectively.

3) The Windkessel model also assumes $R_w(t)/R_w(0)=(V(0)/V_w(t))^{\alpha}$,

where Rw is the resistance in the Windkessel compartment.

4) The arterial volume changes are related to the arterial resistance changes.

In the relationships given above, β represents the vascular compliance, α=2 indicates laminar flow with the vessel, A is a constant and equal to $Vw(0)/(F(0)Rw(0))^{1/\beta}$. With these definitions and initial conditions, the Windkessel model then arrives at the coupled differential equations, (1) and (2), for flow and volume changes due to arterial resistance changes, i.e.

$$\frac{\partial V_w(t)}{\partial t} = F_{in}(t) - F_{out}(t) = F_{in}(t) - \frac{V_w(t)^{\alpha+\beta}}{A^{\beta} R_w(0) V(0)^{\alpha}} \quad (1)$$

$$F_{in}(t) = \frac{P - P_w(t)}{R_A(t)} = \frac{P - V_w(t)^{\beta} / A^{\beta}}{R_A(t)} \quad (2)$$

In this study, we assume a bi-phasic model for the temporal response of arterial resistance during hyperoxic gas intervention according to the bi-phasic behavior of hemodynamic responses to oxygen or carbogen intervention, i.e.

$$R_A = R_{A,f}(0)\exp(-\frac{t-t_0}{\tau_f}) + R_{A,s}(0)\exp(-\frac{t-t_0}{\tau_s}) \quad (3)$$

where $R_{A,f}$ and $R_{A,s}$ are the amplitudes of fast and slow arterial resistance components, τ_f and τ_s are the time constants of fast and slow component, respectively, and t_0 is the time when the rats were exposed to the hyperoxic gas intervention. The numerical solutions of these differential equations, (1) and (2), then provide the relationship between blood flow and blood volume. The units are normalized as $F_{in}(0)=F_{out}(0)=1$, $V_w(0)=F_{in}(0)\tau$, and $R_A(0)+R_w(0)=1$.

In order to estimate the blood flow from blood volume changes, we must assume a constant value of hematocrit during the intervention so that we will have the relationship of $\Delta[HbT]/[HbT]_0=\Delta BV/BV_0$. Based on the Windkessel model, four parameters for the arterial resistance, i.e., $R_{A,f}(0)$, $R_{A,s}(0)$, τ_f and τ_s, need to be quantified besides the Windkessel vascular reserve β and the Windkessel transit time τ. The model parameters were determined or optimized in a nonlinear fit to the experimentally measured Δ[HbT]. Given the optimal parameters, the Windkessel model permits to estimate $\Delta TBF/TBF_0$, which is the function of arterial resistance (R_A), β and τ.

Step 2: Ratio method to estimate $\Delta TMRO_2$

Ratio method has been used to calculate the change in cerebral metabolic rate of oxygen (Jones *et al* 2001). Here we will use the same method, with the C (cerebral) replaced by T (tumor) in equation 4:

$$(1+\frac{\Delta TMRO_2}{TMRO_{2_0}}) = (1+\frac{\Delta TBF}{TBF_0})\cdot(1+\gamma\frac{\Delta Hb}{Hb_0})/(1+\gamma_T\frac{\Delta HbT}{HbT_0}) \quad (4)$$

where γ and γ_T represent the relative changes of deoxy-hemoglobin and total hemoglobin concentration in all vascular compartments, respectively. In our study, Δ[HbT] and Δ[Hb] are measured by NIRS, while ΔTBF can be estimated from the Windkessel model. Then, eq. (4) will further allow us to compute an estimate for changes in $TMRO_2$.

Step 3: Estimation of blood flow and $\Delta TMRO_2$ of rat breast tumors under intervention

There were totally 11 rats under investigation. Group 1 (n=6) was under air-oxygen inhalation, shile group 2 (n=5) had air-carbogen intervention. Figure 1 shows an example of time course of tumor Δ[HbT] and $\Delta[HbO_2]$. $R_{A,f}$ and $R_{A,s}$, the amplitudes of fast and slow arterial resistance change in response to interventions, are equal to 0.19 and 0.6 respectively. The two thick curves were obtained by averaging six sets of measurements from the rat tumors in group 1 when the rats were subject to oxygen intervention. Both Δ[HbT] and $\Delta[HbO_2]$ have stable baselines when the rats were breathing air. When the gas was switched to oxygen, both parameters increased consistently with the typical bi-phasic pattern. ΔTBF was estimated from Δ[HbT], based on the Windkessel model as shown in eqs. (1) to (3); then, $\Delta TMRO_2$ was obtained using eq. (4). Both ΔTBF and $\Delta TMRO_2$ have exhibited significant increases with a bi-phasic pattern too.

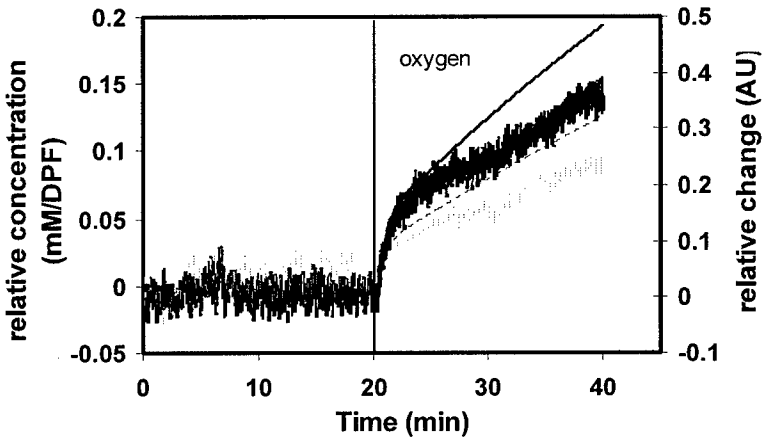

Figure 1. Time course of averaged values of Δ[HbT] (light thick curve), $\Delta[HbO_2]$ (dark thick curve), with fitted ΔTBF (thin dotted curve) and $\Delta TMRO_2$ (thin dark curve), taken from six tumors with gas intervention of air-oxygen. The units of Δ[HbT] and $\Delta[HbO_2]$ are mM/DPF, and the fitted ΔTBF and $\Delta TMRO_2$ have arbitrary units.

However, the tumors have various responses of Δ[HbT], ΔTBF, and $\Delta TMRO_2$ to carbogen inhalation (Fig 2 to 4), while tumor $\Delta[HbO_2]$ always gave consistent increases with given carbogen intervention (Fig 2 to 4). Figure 2 shows the time course of averaged $\Delta[HbO_2]$, Δ[HbT], computed ΔTBF and $\Delta TMRO_2$ from three tumors in group 2 (tumor #1~3) when the rats were subject to the gas intervention. In this case, there is a consistent increase of $\Delta[HbO_2]$ and Δ[HbT]. Estimated from Δ[HbT] using the Windkessel model, $R_{A,f}$ and $R_{A,s}$ are equal to 0.2 and 0.6 respectively, ΔTBF was elevated, and so was the corresponding $\Delta TMRO_2$. However, Δ[HbT] taken from Tumor #4 from group 2 did not show much change, and neither did ΔTBF and $\Delta TMRO_2$ from this tumor in response to carbogen inhalation (Figure 3), while the fitted $R_{A,f}$ and $R_{A,s}$ are equal to 0.05 and 0.05 respectively. Furthermore, Tumor #5 in group 2 shows a decreased Δ[HbT] induced by carbogen intervention, with reduced ΔTBF and $\Delta TMRO_2$ accordingly (Figure 4), and the fitted $R_{A,f}$ and $R_{A,s}$ are equal to 0.45 and 0.5 respectively.

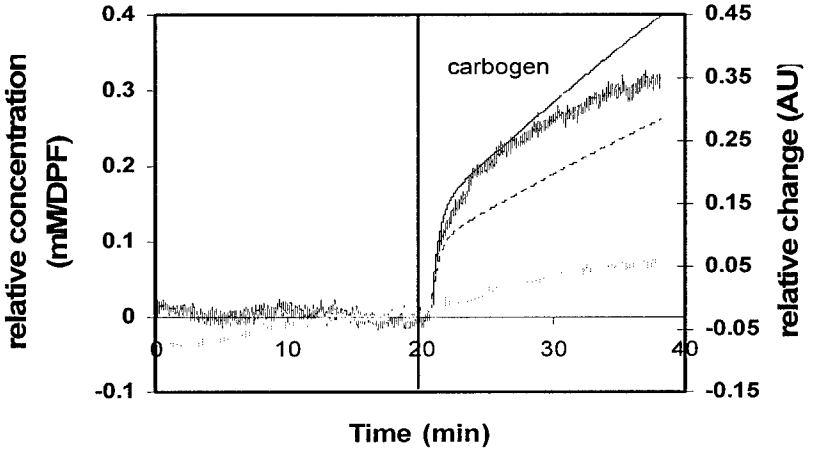

Figure 2. Time course of average values of Δ[HbT] (light thick curve), $\Delta[HbO_2]$ (dark thick curve), with fitted ΔTBF (thin dotted curve) and $\Delta TMRO_2$ (thin dark curve), from three tumors with gas interventions of air-carbogen. The units of Δ[HbT] and $\Delta[HbO_2]$ are mM/DPF, and the fitted ΔTBF and $\Delta TMRO_2$ have arbitrary units.

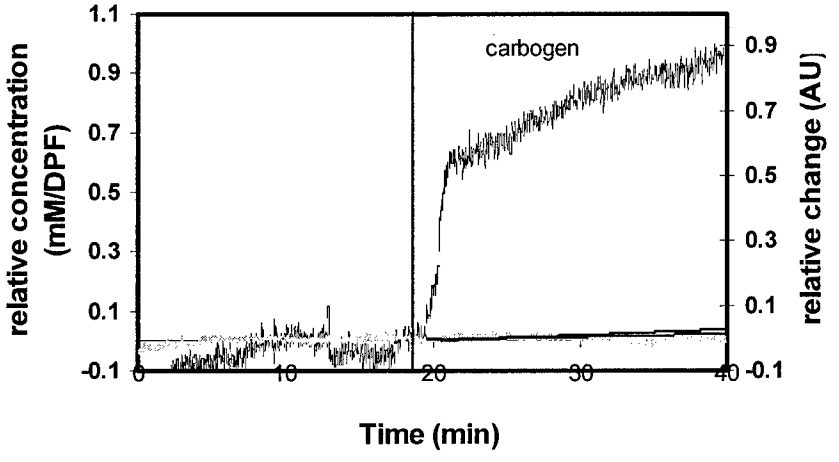

Figure 3. Time course of Δ[HbT], $\Delta[HbO_2]$, computed ΔTBF and $\Delta TMRO_2$ from Tumor 4 of group 2 with air-carbogen intervention.

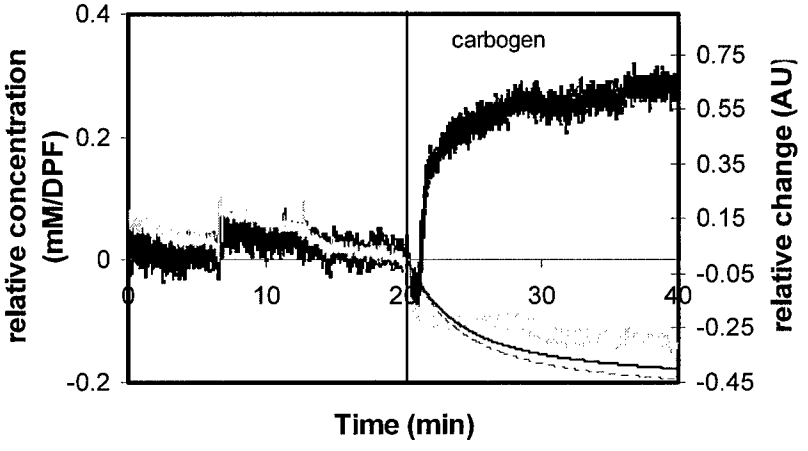

Figure 4. Time course of Δ[HbT], $\Delta[HbO_2]$, computed ΔTBF and $\Delta TMRO_2$ from Tumor 5 of group 2 with air-carbogen intervention.

Task 2: to obtain the knowledge and appropriate training for handling laboratory animals and performing the measurements. (months 9-14)

a. To have training in handling laboratory animals.
b. To study the fundamentals and operation of the 1-channel and 3-channel NIRS system.
c. To study the fundamentals and operation of FOXY fiber optic oxygen sensor.
d. To study the fundamentals and operation of ^{19}F MR EPI imaging.
e. To study the fundamentals and operation of hyperbaric chamber.

The PI has obtained the knowledge and training for handling laboratory animals and performing the measurements. The PI has also studied the fundamentals and operations of multi-channel FOXY oxygen sensor, multi-channel broadband diffuse NIR spectroscopy, and ^{19}F EP imaging and hyperbaric chamber.

Task 3: to study the influence of four different gas interventions on tumor oxygenation using both single-channel NIRS and FOXY system, on various rat breast tumor size. (months 14-30)

The PI has made tremendous efforts to have the fiber probes ready for both the NIR system and FOXY oxygen sensor as well as to integrate the probes with the hyperbaric chamber. We implemented single-channel NIRS with broadband diffuse spectroscopy (BDS) because BDS provides a broad spectrum from 400 to 900 nm, enabling us to calculate the absolute values of hemoglobin concentration with the algorithm that we are currently developing. Being portable, BDS consists of a tungsten halogen light source (HL-2000HP, ocean optics, FL), a hand-held spectrometer (USB2000, Ocean optics, FL), and two optical fiber bundles with respective 2.6 mm and 1 mm bundle diameter. The current design of the fibers provides us with better optical transmittance without sacrificing their compatibility of light source and spectrometer.

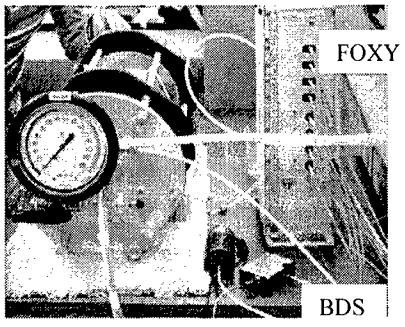

Figure 5. Picture of hyperbaric chamber (left one), integrating with broadband light diffuse spectroscopy source and detector probes (white ones) and FOXY oxygen sensor probes (blue ones), FOXY oxygen sensor (right one) and BDS (middle ones)

As shown in Figure 5, the hyperbaric chamber is made of transparent acrylic, which allows direct visualization during experiments. The chamber is cylinder-shaped with an inner diameter of 8 inch and a length of 24 inch. One end is attached with a removable door, and the other end is fixed, on which a pressure meter and gas inlet and outlet valves are integrated to monitor and control the pressure and gas flow rate in the chamber. Optical fiber probes of BDS and FOXY were assembled into the chamber, while the instruments themselves were placed outside the chamber to avoid any possible fire hazards (Figure 5).

Because safety is a very important consideration for hyperbaric chamber (Jain 1999), all facilities required in the chamber are specially designed to avoid any possibility of fire hazard. The optical probe ends were made of plastic instead of metal to avoid static electricity, which may be produced by the friction between the probe and probe holder. The homemade optical breadboard inside the chamber is made of acrylic plastic, with two fixing tubes attached on both sides to assure the stability of the board sitting in the cylindrical chamber. All metal probe holders were washed thoroughly to remove all lubricate oil.

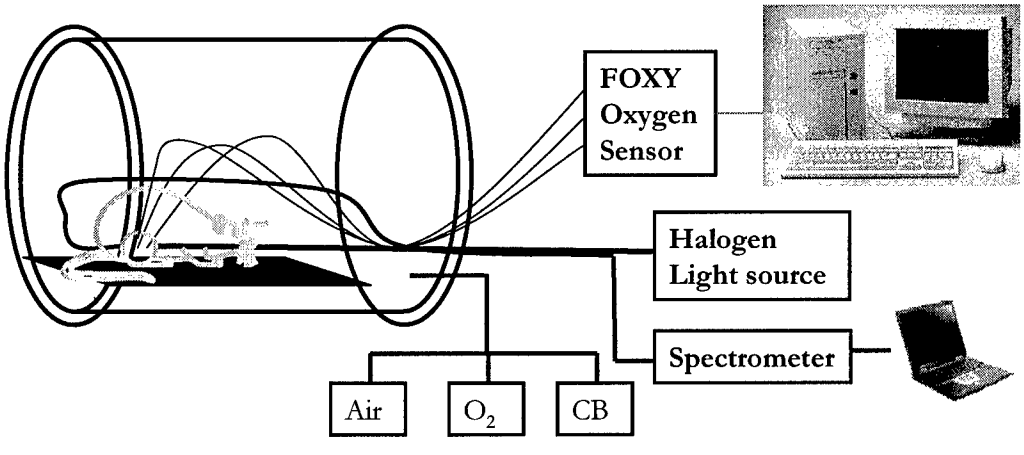

Figure 6. Schematic diagram of experimental setup for simultaneous monitoring of tumor vascular and tissue oxygenation when the rats are under hyperbaric gas

A Fisher 344 rat was placed in the hyperbaric chamber before the experiment, as shown in figure 6. The

probe ends of source and detector bundles of BDS were placed on the opposite side of the tumor in transmission geometry. Three needle probes of the FOXY oxygen sensor were inserted into different regions of the tumor. The rat was exposed to varying gas environment according to the following challenge paradigms:

Air (15min) → Oxygen (1 ATA, 15 min) → Oxygen (2 ATA, 30 min) → Air (30 min)

where ATA stands for 1 atmosphere absolute.

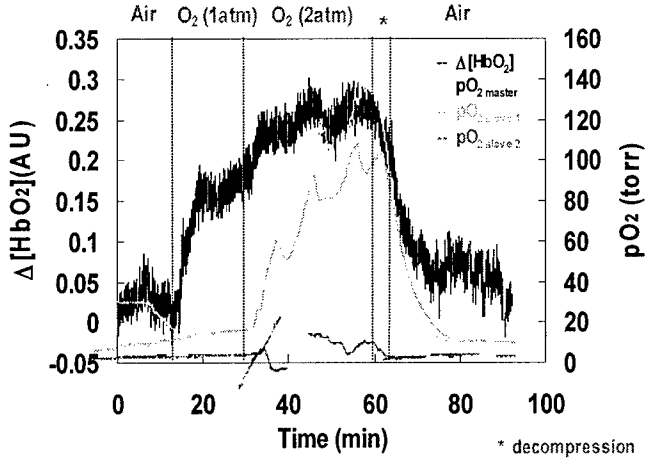

Figure 7 Temporal profiles of $\Delta[HbO_2]$ and pO_2 in response to respiratory challenge for a rat breast tumor, measured simultaneously by both BDS and FOXY oxygen sensor. $pO_{2\_master}/pO_{2\ slave1}/pO_{2\ slave2}$ represent pO_2 readings from three different regions of the tumor (region 1, 2, 3).

Figure 7 shows $\Delta[HbO_2]$ and pO_2 responses to respiratory challenge simultaneously measured by BDS and FOXY, respectively. Baseline measurements (breathing air) were generally stable in $\Delta[HbO_2]$, and altering the inhaled gas to oxygen in 1 atmosphere absolute (ATA) induced a rapid and significant increase, followed by a gradual change in $\Delta[HbO_2]$. Changing the gas to hyperbaric oxygen in 2 ATA leads to additional improvement of $\Delta[HbO_2]$. Upon return to air (baseline), $\Delta[HbO_2]$ dropped quickly first and more gradually later. Comparatively, not all regional pO_2 show stable baseline: pO_2 in region 1 shows the stable value in the first 10 min, but it has a gradual decrease in the following 5 min, while pO_2 in regions 2 and 3 remain unfaltering in air. When the gas was switched to oxygen (1 ATA), pO_2 in region 1 increase gradually, while pO_2 in regions 2 and 3 do not show much significant improvement. Further changing the gas to hyperbaric oxygen (2 ATA) causes substantial improvement of pO_2 in all three local regions. Upon return to air, pO_2 in regions 1 and 2 return to baseline gradually, while that in region 3 drops to baseline quickly.

Key Research Accomplishments

1) The PI had developed a mathematic model to correlate the hemoglobin concentration to blood flow and metabolic rate of oxygen in tumor. We demonstrated that we are able to quantify the tumor blood flow and metabolic rate of oxygen based on the measurement of hemoglobin

concentration using NIRS during gas intervention.

2) The PI has obtained the knowledge and training for handling laboratory animals and performing initial animal measurements independently using multi-channel FOXY oxygen sensors, broadband diffuse NIR spectroscopy, ^{19}F EPI imaging and a hyperbaric chamber.
3) The PI has designed and implemented fiber probes ready for both the NIR system and FOXY pO_2 system, and integrated the probes with the hyperbaric chamber. She had gotten preliminary data of the simultaneous measurement under hyperbaric oxygenation, which is supposed to accomplish in the second year.

Reportable Outcomes:

Peer-reviewed Journal:

1) **Mengna Xia**, Vikram Kodibagkar, Hanli Liu and Ralph Mason, "Tumor oxygen dynamic measured simultaneously by near infrared spectroscopy and ^{19}F magnetic resonance imaging in rats", under 2nd review of Physics in Medicine and Biology.
2) Jae Kim, **Mengna Xia,** Hanli Liu, "Extinction coefficients of hemoglobin for near-infrared spectroscopy of tissue", IEEE Engineering in Medicine and Biology magazine, 24: 118-121 (2005)
3) Yueqing Gu, Wei R. Chen, **Mengna Xia**, Sang W. Jeong, and Hanli Liu, " Effect Of photothermal therapy On breast tumor vascular contents: non-invasive monitoring by near infrared spectroscopy", Photochemistry and Photobiology, in press, 2005

Presentation and Proceeding Papers:

1) **Mengna Xia**, Vikram Kodibagkar, Ralph Mason, Benjamin Levine, Hanli Liu, "Tumor vascular and tissue oxygenation dynamics under normobaric and hyperbaric oxygen interventions", presented at the fourth Era of Hope meeting for the Department of Defense (DOD) Breast Cancer Research Program (BCRP) held on June 8-11, 2005 in Philadelphia, Pennsylvania
2) **Mengna Xia**, Ralph Mason, Hanli Liu, "A model of hemodynamic responses of rat tumors to hyperoxic gas challenge", Proc. SPIE- Optical Tomography and Spectroscopy of Tissue VI, 5693: 301-307 (2005)
3) **Mengna Xia**, Vikram Kodibagkar, Yueqing Gu, Anca Constantinescu, Ralph Mason, Hanli Liu, "Tumor oxygen dynamics measured simultaneously by near infrared spectroscopy and ^{19}F MR EPI imaging", in Biomedical Topical Meetings on CD-ROM (The Optical Society of America, Washington, DC, 2004), ThF33
4) Yueqing Gu, Vikram Kodibagkar, **Mengna Xia**, Anca Constantinescu, Ralph P. Mason, Hanli Liu, "Breast tumor vascular oxygenation and blood volume assessed by near-infrared spectroscopy and magnetic resonance", Proc. SPIE- Optics in Health Care and Biomedical Optics: Diagnostics and Treatment II, 5630: 918-925 (2004)

Conclusions:

Up to date, we could draw the following conclusions from the work that we have conducted in Year 1:

1) We estimated the hyperoxic gas induced tumor blood flow changes by fitting the model to the measured Δ[HbT]. The bi-phasic feature of the fitted blood flow is consistent with the

hypothesis that there exist two distinct regions within a tumor: 1) a well perfused region with a regular blood flow, and 2) a poorly perfused region with slow blood flow (*** references of my Applied Optics paper and Jae's Optics Express paper). Mathematically, the bi-phasic feature of blood volume (i.e., total hemoglobin concentration) change during hyperoxic gas intervention provides a connection between the computational model and our experimental tumor data. We believe that the hemodynamic parameters, such as $\Delta[HbO_2]$, $\Delta[Hb]$ and $\Delta[HbT]$ directly measured from NIRS, ΔTBF and $\Delta TMRO_2$ indirectly estimated from NIRS, can provide valuable insight into the tumor compartment of such a complex system and allow us to explore dynamic signatures of tumours. All of these can, in turn, enhance/assist human cancer diagnosis and prognosis. Overall, NIRS is a noninvasive tool to monitor tumor oxygenation and may also serve as a mediator to estimate tumor perfusion and oxygen consumption rate with response to intervention in tumor tissue.

2) Normobaric hyperoxic gas (oxygen and carbogen) can effectively manipulate the vascular oxygen level in breast tumors. However, different regions in a tumor show heterogenous responses to normobaric oxygen inhalation. Hyperbaric oxygen is shown to improve both the tumor vascular and tissue oxygen level more effectively than normobaric oxygen.

Reference:

Boas D, Strangman G, Culver J, Hoge R, Jasdzewski G, Poldrack R, Rosen B and Mandeville J 2003 Can the cerebral metabolic rate of oxygen be estimated with near-infrared spectroscopy? *Phys Med Biol* **48** 2405-18

Jain K K 1999 hyperbaric chambers: equipment, technique, and safety *Textbook of hyperbaric medicine* ed K K jain (Seattle: Hogrefe & Huber)

Jones M, Berwick J, Johnston D and Mayhew J 2001 Concurrent Optical Imaging Spectroscopy and Laser-Doppler Flowmetry: The Relationship between Blood Flow, Oxygenation, and Volume in Rodent Barrel Cortex *NeuroImage* **13** 1002-15

Mandeville J, Marota J, Ayata C, Zaharchuk G, Moskowitz M, Rosen B and Weisskoff R 1999 Evidence of a cerebrovascular postarteriole windkessel with delayed compliance *J Cereb Blood Flow Metab* **19** 679-89

Appendix:

Manuscript under second review of *Physics in Medicine and Biology*

Tumour oxygen dynamics measured simultaneously by near infrared spectroscopy and ^{19}F magnetic resonance imaging in rats[+]

Mengna Xia[1], Vikram Kodibagkar[2], Hanli Liu[1], Ralph P. Mason[1,2,*]

[1]Joint Biomedical Engineering Graduate Program,

University of Texas at Arlington/University of Texas Southwestern Medical Center at Dallas, TX 76019

[2]Cancer Imaging Program, Department of Radiology,

University of Texas Southwestern Medical Center at Dallas,

TX 75390

* Corresponding author:
Ralph P. Mason, Ph.D., CSci, CChem.,
Department of Radiology,
U.T. Southwestern Medical Center,
5323 Harry Hines Blvd.,
Dallas, TX 75390-9058
Tel: (214) 648-8926; Fax: (214) 648-2991;
E. mail: Ralph.Mason@UTSouthwestern.edu

Running title: Tumour oxygen dynamics in vasculature and tissue

Tumor oxygen dynamics by simultaneous NIRS and ^{19}F MRI in rats

[+]Presented in part at the 12th annual meeting of the International Society of Magnetic Resonance in Medicine, Kyoto, 2004

Tumor oxygen dynamics by simultaneous NIRS and ^{19}F MRI in rats

Abstract

Simultaneous near-infrared spectroscopy (NIRS) and magnetic resonance imaging (MRI) were used to investigate the correlation between tumour vascular oxygenation and tissue oxygen tension dynamics in rat breast 13762NF tumours with respect to hyperoxic gas breathing. NIRS directly detected global variations in the oxygenated haemoglobin concentration ($\Delta[HbO_2]$) within tumours and oxygen tension (pO_2) maps were achieved using ^{19}F MRI of the reporter molecule hexafluorobenzene. Multiple correlations were examined between rates and magnitudes of vascular ($\Delta[HbO_2]$) and tissue (pO_2) responses. Significant correlations were found between response to oxygen and carbogen breathing using either modality. Comparison of results for the two methods showed a correlation between the vascular perfusion rate ratio and the mean pO_2 values ($R^2>0.7$). The initial rates of increase of $\Delta[HbO_2]$ and the slope of dynamic pO_2 response, $d(pO_2)/dt$ of well oxygenated voxels in response to hyperoxic challenge were also correlated. These results demonstrate the feasibility of simultaneous measurements using NIRS and MRI. As expected, the rate of pO_2 response to oxygen is primarily dependent upon the well-perfused rather than poorly perfused vasculature.

Keywords: Near infrared spectroscopy, Magnetic resonance imaging, Breast tumour, Oxygenation, Haemoglobin, Hexafluorobenzene.

1. Introduction

Tumour oxygenation has been widely recognized as a pivotal factor in the efficacy of radiotherapy (Hall 1994), photodynamic therapy (Chapman *et al* 1991) and some chemotherapies (Brown 1999) and patient stratification with respect to tumour oxygenation status could be clinically important (Hockel *et al* 1996, Fyles *et al* 1998, Welch *et al* 2003). It has been hoped that modulation of tumour oxygenation could be applied to enhance therapeutic efficacy. An attractive intervention is breathing hyperoxic gas, and indeed, several clinical trials have examined the efficacy of normobaric or hyperbaric oxygen, to improve therapeutic outcome, but often with marginal success (Overgaard and Horsman 1996). It has been suggested that outcome might have been improved, if responsive tumours could have been identified *a priori.* Accordingly, accurate evaluation of tumour oxygenation in response to interventions at various stages of growth should provide a better understanding of tumour response to therapy, potentially allowing therapy to be tailored to individual characteristics.

Given the importance of tumour oxygenation, many techniques have been developed based on microelectrodes, optical reflectance, Electron Paramagnetic Resonance (EPR), Magnetic Resonance Imaging (MRI) and nuclear medicine approaches, as reviewed previously (Mason *et al* 2002, Zhao *et al* 2004). While each approach has unique strengths, some are highly invasive. Near-infrared spectroscopy (NIRS) has been developed in recent years as a promising non-invasive technique to quantify the concentration of tissue chromophores, such as oxygenated and deoxygenated haemoglobin, water and lipid (Sevick *et al* 1991, Liu *et al* 2000). Due to the deep penetration depth and biochemical specificity of NIRS, it has been widely applied for quantitative measurements of cerebral oxygenation (Delpy and Cope 1997, Yodh and Boas 2003) and blood oxygenation in muscles *in vivo* (Homma *et al* 1996). Recently, NIRS has been also used to monitor tumour vascular oxygenation with respect to interventions (Hull *et al* 1999, Liu *et al* 2000, Gu *et al* 2003). With notable exceptions (Chance 1997, Dehghani *et al* 2004, Shah *et al* 2004, Pogue *et al* 2003), NIRS currently lacks spatial resolution, and thus, the utility of global measurements requires validation, given the well-documented heterogeneity of tumour oxygenation. In this regard, Conover *et al* (2000) compared the spatially averaged measurement of tumour oxygen

saturation (SO_2) using NIRS with the local SO_2 reading in individual blood vessels measured by cryospectrophotometry. The sensitivity and specificity analysis suggests that NIRS may identify clinically relevant hypoxia, even when its spatial extent is below the resolution limit of the NIRS technique. We have previously investigated correlates between pO_2 assessed by electrodes (Mason *et al* 2003, Kim *et al* 2003b) or fibre-optic probes and NIRS (Gu *et al* 2003). On occasion, there was a good correlation between global vascular oxygenation assessed and local pO_2 at individual locations, but often, disparate behaviour was observed. Sequential MRI and NIRS suggested a better relationship based on average pO_2 from multiple locations (Kim *et al* 2003b). We have now implemented simultaneous NIRS and ^{19}F MRI to examine the relationships further. Since NIRS is entirely non-invasive it would provide an attractive surrogate for monitoring tumour oxygenation, and hence, we seek correlations with absolute pO_2 measurements observed simultaneously by MRI.

2. Materials and methods

Investigations were approved by the Institutional Animal Care and Use Committee.

2.1. Animal preparation and experimental set-up

Mammary adenocarcinomas 13762NF (cells originally obtained from the Division of Cancer Therapeutics, NCI) were implanted in skin pedicles (Hahn *et al* 1993) on the foreback of ten adult female Fisher 344 rats weighing ~150 g. When the tumours reached ~1 cm in diameter, the rats were anaesthetised with ketamine hydrochloride i.p. (100 mg/kg body weight, Aveco, Fort Dodge, IA) and were maintained under general gaseous anaesthesia (air and 1% isoflurane; Baxter International Inc, Deerfield, IL). Tumour hair was trimmed to give good optical contact for NIR light transmission. Hexafluorobenzene (HFB, 50 µl, 99.9%, Lancaster Co., Pelham, NH) was administered along two or three tracks in central and peripheral regions of the tumours in a single plane (transverse to the rat's tumour, and in the region of NIR photon pathway) using a Hamilton syringe with a 32 G needle. The needle was inserted manually to penetrate across the tumour and was withdrawn ~1 mm to reduce

pressure and 3~4 μl of HFB were deposited. The needle was then repeatedly withdrawn 1~2 mm and further HFB deposited at each point, as described in detail previously (Zhao *et al* 2004).

The tumour was placed inside a size-matched Helmholtz coil, specially designed for the simultaneous MRI-NIRS study. The tumour was inserted between the two loops of the Helmholtz coil and two NIRS probes were introduced through the ends of the coil along the coil axis (figure 1). The probes were positioned to be in the same plane as the HFB injection. The rats were placed in the magnet on their side, and body temperature was maintained using a warm water blanket. A total of ten rats were used in the study: seven rats were subjected to respiratory challenge in the sequence of air-oxygen-air-carbogen-air, one rat breathed air-carbogen-air-oxygen-air, one rat breathed air-carbogen-air, and the last one breathed air-oxygen-air.

2.2. NIRS for measuring $\Delta[HbO_2]$

A homodyne frequency-domain system (NIM, Philadelphia, PA) was used to monitor the global change of deoxy- and oxy-haemoglobin concentration ($\Delta[HbO_2]$) in the tumour, as described previously (Yang *et al* 1997), though with minor modifications to ensure MR compatibility (figure 1). Briefly, the laser light, which was emitted from two laser diodes (at 758 nm and 785nm), was amplitude-modulated at 140 MHz and time gated on and off sequentially. The two time-shared laser beams illuminated the tumour surface alternately through a light-delivery fibre bundle (source fibre) with a 7-meter length and a 3-mm bundle diameter. The long fibre bundle ensured the separation of the NIRS hardware from the magnet. After being absorbed and scattered in the tumour tissue, the transmitted light was collected on the opposite side of the tumour by another fibre bundle of same length and diameter (detector fibre) as those of source fibre. The collected optical signal was then detected and amplified by a photomultiplier tube (PMT). The source and detector fibre bundles are shown in figure 1, and both of the probe sheaths at the fibre tips were made of nylon for MR compatibility. An In-phase and Quadrature (I/Q) demodulator chip was used to demodulate the amplitude-modulated signal from the PMT.

In principle, since the I/Q system could give both phase and amplitude values, we should be able to obtain absolute calculations of HbO_2, Hb, and SO_2 (Yang *et al*, 1997). However, given the tumor's small size and large spatial heterogeneity, it is very difficult to obtain such absolute quantification accurately using the conventional algorithm (Fishkin and Gratton 1993) based on the diffusion approximation. Instead, based on modified Beer-Lambert's law, we can use the amplitude of the light transmitted through the tumor to calculate concentration changes in HbO_2, Hb, and Hb_t of the tumor caused by respiratory intervention. Namely, changes of oxy- and deoxy-haemoglobin concentration, $\Delta[HbO_2]$ and $\Delta[Hb]$, respectively, can be derived from the measured amplitudes at the two wavelengths (758 nm and 785 nm) (Kim *et al* 2003b)

$$\Delta[HbO_2] = \frac{-10.63\log(\frac{A_b}{A_t})^{758} + 14.97\log(\frac{A_b}{A_t})^{785}}{DPF \cdot d} \quad (1)$$

$$\Delta[Hb] = \frac{8.95\log(\frac{A_b}{A_t})^{758} - 6.73\log(\frac{A_b}{A_t})^{785}}{DPF \cdot d} \quad (2)$$

where A_b is the baseline amplitude, A_t is the transient amplitude during measurement, and d is the direct source-detector separation. *DPF* (differential path-length factor) is a tissue-dependent parameter and is defined as the ratio between the optical path length and the physical separation between the source and detector. Notice that the units for $\Delta[HbO_2]$, $\Delta[Hb]$, and $\Delta[Hb]_{total}$ are mM. Since *DPF* is a variable, depending on tissue types and wavelengths, it is currently difficult to quantify *DPF* for tumours. Because our study focuses on dynamic changes of $[HbO_2]$, $\Delta[HbO_2]$ values may be scaled by a factor of DPF, in the unit of mM/DPF, to obtain characteristic features of tumour oxygen dynamics (Liu *et al* 2000).

2.3. Mathematical model for blood oxygenation dynamics of tumours

Based on our previous experimental study, we derived a simple mathematical model (Liu *et al* 2000) to examine tumour vascular dynamics during oxygen intervention, by analogy to the method used to quantify regional cerebral blood flow (rCBF) with diffusible radiotracers, originally developed by Kety

(1951). Accordingly, changes of oxy-haemoglobin concentration in tumour vasculature induced by hyperoxic gas intervention, $\Delta[HbO_2]$, could be expressed as

$$\Delta[HbO_2(t)]^{vasculature} = \gamma H_0[1-\exp(-\frac{ft}{\gamma})] = A[1-\exp(-\frac{t}{\tau})] \quad (3)$$

where $\Delta[HbO_2]$ corresponds to the changes in oxy-haemoglobin concentration from tumour vasculature measured by the NIRS, H_0 is the arterial oxygenation input for ΔHbO_2^{artery} after time 0, f is the blood perfusion rate, and γ is the ratio of $[HbO_2]$ changes in the vascular bed to that in the veins and defined as vascular coefficient of the tumour. Specifically, $\gamma = \Delta[HbO_2]^{vasculature}/\Delta[HbO_2]^{vein}$, τ is the time constant ($=\gamma/f$), and $A=\gamma H_0$.

Given the fact that solid tumours often develop hypoxic regions which are poorly perfused in the centre as they grow (Mazurchuk *et al* 1999, Song *et al* 2002), we hypothesized that the observed, bi-phasic feature of $\Delta[HbO_2]$ came from two different perfusion regions in tumours (well-perfused and poorly perfused region). Therefore, it is reasonable to define two different blood perfusion rates (f_1, f_2) with two different vascular coefficients (γ_1, γ_2) in the mathematical model. Consequently, eq.3 has been modified to a summation of two exponential expressions, representing two perfusion regions, as

$$\begin{aligned}\Delta[HbO_2(t)]^{vasculature} &= \gamma_1 H_0[1-\exp(-\frac{f_1 t}{\gamma_1})] + \gamma_2 H_0[1-\exp(-\frac{f_2 t}{\gamma_2})] \\ &= A_1[1-\exp(-\frac{t}{\tau_1})] + A_2[1-\exp(-\frac{t}{\tau_2})] \quad (4)\end{aligned}$$

where f_1 and γ_1 are the blood perfusion rate and the vasculature coefficient, respectively, in the well-perfused region, and f_2 and γ_2 represent the same respective meanings in the poorly perfused region. Also, it follows that $A_1=\gamma_1 H_0$, $A_2=\gamma_2 H_0$, $\tau_1=\gamma_1/f_1$ and $\tau_2=\gamma_2/f_2$. Since A_1, A_2, τ_1, and τ_2 can be determined by curve-fitting equation (4) to the dynamic NIRS measurements, we can obtain the ratios for two vascular coefficients and two blood perfusion rates, as follows (Liu *et al* 2000):

$$\frac{\gamma_1}{\gamma_2} = \frac{A_1}{A_2}, \qquad \frac{f_1}{f_2} = \frac{A_1/\tau_1}{A_2/\tau_2}. \tag{5}$$

These two ratios enable us to understand more about tumour vascular structures and blood perfusion rates. Namely, γ_1/γ_2 may be associated with the vascular volume fraction between the two regions, and f_1/f_2 reflects the perfusion ratio between the two regions. For example, if f_1/f_2 is substantially greater than 1, the two compartments have significantly different perfusion rates.

This mathematical model has been utilized well to explain our experimental animal studies (Liu *et al* 2000, Gu *et al* 2003, Kim *et al* 2003b). Moreover, it has been supported by computer simulations (Kim and Liu 2005) and phantom study (Kim and Liu 2004) that the bi-phasic or bi-exponential feature can be well present if both a slow and a fast perfusion of flow co-exist within the interrogated area or volume by the NIR source and detector. In this paper, our theoretical analysis is also based on the same mathematical model, as given in equations (4) and (5).

2.4. FREDOM for measuring pO_2

MRI experiments were performed using a Varian Inova 4.7 T horizontal bore system equipped with actively shielded gradients. Shimming was performed on the tumour tissue water signal to reduce the line-width to less than 100 Hz. ^{1}H MRI (200.1 MHz) T1-weighted reference images were acquired with TR/TE of 150/10 ms and 40x40 mm^2 field of view. Following ^{1}H MRI, corresponding ^{19}F MR images (188.3 MHz) with a matrix size of 32x32 (1.25 mm per pixel) were obtained to show the distribution of HFB in the tumour. A single 4-mm thick slice was chosen to include all of the injected HFB as the plane of injection may not be perfectly aligned with the imaging plane. The *FREDOM* (*F*luorocarbon *R*elaxometry by *E*cho-planar imaging for *D*ynamic *O*xygen *M*apping) approach was used to measure pO_2, as described in detail previously (Hunjan *et al* 2001). The spin lattice relaxation rate (R1= 1/T1) of HFB is highly sensitive to changes in pO_2, but not sensitive to temperature variations: a deviation of 1 °C in temperature will introduce a deviation of only 0.13 torr in pO_2 estimate, when pO_2 is about 5 torr (Zhao *et al* 2004). T1 maps were computed on a voxel-by-voxel basis using non-linear least-squares data fitting

by the Gauss-Newton method. We applied a threshold to the raw T1 data in order to remove random noise, *i.e.*, voxels with T1 error >3.6 sec or T1 error/T1 >50% were disregarded. Maps of pO_2 values with 1.25 mm pixel size were obtained from the T1 maps using the equation, $pO_2 = (1/T1-0.0835)/0.001876$ (Hunjan *et al* 2001).

Each pO_2 map took 6 and 1/2 minutes to acquire. Three baseline pO_2 data sets were acquired over 24 mins for all tumours, while the rats breathed air, after which the rats were repeatedly exposed to oxygen or carbogen (95% O_2 and 5% CO_2) interventions. Five pO_2 maps were obtained during each subsequent gas switch period. Typically, for a five gas-intervention sequence (*e.g.*, air-oxygen-air-carbogen-air), a total of 23 pO_2 maps were obtained over a period of 3 h. Due to thresholding, some voxels did not appear in all pO_2 maps and these were discarded. For temporal analysis, voxels were selected as only those which provided consistently reliable data (*i.e.*, satisfied all the thresholding criteria specified above) for all 23 measurements over the time course with a range of 5 to 44 acceptable voxels for the ten tumours. The slope of dynamic pO2 changes (rate) was defined as $d(pO_2)/dt$ and $d(pO_2')/dt$ in response to increasing or decreasing inhaled FO_2 (Fraction of O_2), respectively.

2.5. Statistical Analysis

Linear regression analysis was used to calculate the correlation between the NIRS-derived tumour hemodynamic parameters (*i.e.*, $\Delta[HbO_2]$, A_1/τ_1, A_2/τ_2, f_1/f_2) and the *FREDOM*-determined tumour parameters (*i.e.*, pO_2, $d(pO_2)/dt$, $d(pO_2')/dt$). Data are presented as mean ± standard deviation (SD) and paired Student-t tests compared the effects of oxygen and carbogen on $\Delta[HbO_2]$ and pO_2.

3. Results

3.1. Dynamic response of $\Delta[HbO_2]$ measured by NIRS

Figure 2 shows a group-averaged, temporal profile of $\Delta[HbO_2]$ from seven 13762NF rat breast tumours with air-oxygen-air-carbogen-air intervention, displaying apparent biphasic responses to both

interventions. Both single (eq. 3) and double-exponential (eq. 4) curve fitting were tested for the carbogen intervention in one representative tumour (1.6 cm^3), as in figure 3A. The maximal $\Delta[HbO_2]$ achieved with oxygen challenge was compared with that of carbogen, and revealed no significant difference between oxygen and carbogen intervention ($p>0.3$); indeed, there was a strong correlation between the maximal $\Delta[HbO_2]$ values with these two interventions ($R^2>0.75$, figure 3B), consistent with our previous observations (Gu *et al* 2003). No correlation was found between the perfusion rate ratio (f_1/f_2) and tumour size ($R^2=0.16$). Vascular oxygen dynamics in response to interventions are provided for individual tumours as supplementary material.

3.2. pO_2 measurements by FREDOM

Overlay of ^{19}F and ^{1}H MR images demonstrated that HFB was distributed in both central and peripheral regions of tumour (not shown). Individual pO_2 values taken from each voxel ranged from hypoxia (< 1 torr) to 35 torr under baseline conditions (figure 4). Mean baseline pO_2, which are averaged over all voxels in the first three pO_2 maps, ranged from hypoxia (< 5 torr) to 27 torr with a hypoxic fraction (HF_5; fractional voxels that are less than 5 torr) ranging from 0 to 100% (mean 36%) and summarised in table 1. A strong correlation was found between mean baseline pO_2 and HF_5 ($R^2>0.85$, figure 5). Administration of oxygen or carbogen produced significant increases in tumour pO_2, as shown in the pO_2 maps, graphs and table. The tumour pO_2 values shown here are volume-averaged over the entire slice. The pO_2 responses to respiratory challenge from the group of seven tumors, measured simultaneously by *FREDOM* and NIRS, are also shown in figure 2. Baseline measurements (breathing air) were generally stable, and altering the inhaled gas to oxygen or carbogen induced rapid and significant changes in both pO_2 and $\Delta[HbO_2]$ ($p<0.001$). Upon return to air (baseline), $\Delta[HbO_2]$ dropped quickly and significantly within 16 mins, and then more slowly, for the next 24 mins, whereas the pO_2 decrease was more gradual. Altering the inhaled gas to carbogen also produced a rapid increase in both pO_2 and $\Delta[HbO_2]$. Upon return to air breathing from carbogen, both $\Delta[HbO_2]$ and pO_2 showed a similar trend to that following

oxygen. As expected, all ten tumours showed a significant increase in pO_2 (volume average over entire slice), and decrease in hypoxic fraction (HF) in response to oxygen or carbogen inhalation. The magnitude of response to either hyperoxic gas was correlated (R^2>0.79), as was the maximum volume-averaged pO_2 achieved with either gas (R^2>0.83). The rate of increase with oxygen challenge, $d(pO_2)/dt$, was significantly faster than the return to baseline, $d(pO_2')/dt$, for oxygen intervention ($p<0.02$), but no difference was observed for carbogen ($p>0.1$, figure 6). The mean pO_2 values averaged over the final three pO_2 maps during exposure to carbogen breathing were significantly higher than oxygen ($p<0.01$), and the tumour hypoxic fraction was generally eliminated during carbogen breathing (n = 7 of 9 tumours, table 1).

3.3. **The relationship between pO_2 and $\Delta[HbO_2]$ with respect to hyperoxic gas**

Taken as a group of 10 tumours, there was no apparent relationship between the magnitude of the change in tumour vascular oxygenation ($\Delta[HbO_2]$) and change in pO_2 ($R^2<0.1$). However, if tumours were divided into two sub-populations, then two separate correlations were found each with similar slope (figure 7A). There was also a correlation ($R^2>0.7$) between the perfusion rate ratio, f_1/f_2, derived from fitting the $\Delta[HbO_2]$ curve and the mean pO_2 values achieved with hyperoxic gas intervention (figure 7B). Assessment of f_1/f_2 is predicated on biphasic behaviour with respect to interventions, which was observed in most cases (13 of 16 measurements). There was also a positive correlation between A_1/τ_1 (the fast component of biphasic $\Delta[HbO_2]$) and the $d(pO_2)/dt$ of well oxygenated voxels (*i.e.*, those with pO_2 values > 10 torr under oxygen or carbogen intervention) ($R^2>0.5$, figure 8). However, no correlation was found between $d(pO_2)/dt$ and A_2/τ_2 (the slow component).

4. Discussion

Integration of diverse imaging techniques can be technically challenging, since each modality has specific technical constraints and requirements. Here, the NIR system was modified to use longer optical fibres

and any metal components were eliminated from the fibre tips. Due to the spatial restrictions within the bore of the magnet a Helmholtz coil was built specifically providing access to both the tumour and fibres. The fibres required sufficient flexibility to allow them to be bent through requisite angles within the confines of the magnet bore. To date there have been few reports of simultaneous data acquisition by NIR and MRI on phantom (Pogue *et al* 2003), human brain (Toronov *et al* 2001, Chen *et al* 2003) and human breast (Ntziachristos *et al* 2000, Gulsen *et al* 2002, Ntziachristos *et al* 2002, Gu *et al* 2004a).

In the present study, global average $\Delta[HbO_2]$ was measured by NIRS, and pO_2 maps were obtained simultaneously by ^{19}F MRI. We used transmission mode NIRS in order to interrogate deep tumour tissue. While NIRS is a global measurement, the region sampled by it is predominantly a banana-shape region joining the locations of the source and detector (Arridge 1995, Arridge and Schweiger 1995), and we recently showed that typically 15 to 30% of the vascular volumes of rat tumours are interrogated by NIR using this configuration (Gu *et al* 2004b). We positioned the NIRS probes (source and detector) to be in the same plane as the HFB injection to ensure maximum overlap between the regions sampled by the two techniques. Utilising our previously developed mathematical model (Liu *et al* 2000), multiple hemodynamic parameters were derived for $\Delta[HbO_2]$ ($A_1/\tau_1, A_2/\tau_2$ and f_1/f_2) to be compared with pO_2. Our results demonstrate that oxygenation parameters measured from both techniques show significant and consistent elevation in tumour oxygenation during the hyperoxic gas interventions. As reported previously, the magnitude of the vascular response was similar with both hyperoxic gases (Gu *et al* 2003). As expected, $\Delta[HbO_2]$ increased much faster than pO_2 in all ten tumours, indicating that change in tumour vascular oxygenation precedes tumour tissue oxygenation. This observation is consistent with our previous studies in this tumour type measured simultaneously by NIRS and fibre-optic probes (Gu *et al* 2003), as well in the Dunning prostate R3327-AT1 tumours measured sequentially by NIRS and ^{19}F MRI (Kim *et al* 2003b).

We have previously demonstrated the application of *FREDOM* to monitor tumour oxygen dynamics in diverse rat prostate tumours (Zhao *et al* 2001, Zhao *et al* 2002), human tumour xenografts (Mason *et*

al 2002) and a few breast tumours (Song *et al* 2002). Here, mean baseline was pO_2=12 ± 10 torr for the 10 tumours, which is lower than reported previously (Song *et al* 2002), but entirely consistent with the newer anaesthetic protocol (air or 21% oxygen, as opposed to 33% O_2 previously). There was a strong correlation between baseline pO_2 and hypoxic fraction (figure 5), as we have previously found using Dunning prostate R3327-HI tumours (Zhao *et al* 2001). The pO_2 achieved with carbogen in this study was significantly higher than with oxygen and carbogen appeared to be more effective at eliminating the hypoxic fraction. However, carbogen was generally applied second in our experimental protocols, and it is highly likely that the initial oxygen primed the tumour. Indeed, while oxyhaemoglobin generally returned to baseline during the air breathing episode between hyperoxic gases, it is clear that pO_2 remained elevated (figure 2). Both ΔpO_2 and the maximum pO_2 achieved with either gas were closely correlated. Similar behaviour was reported previously based on measurements using fibre optic probes (Gu *et al* 2003). For the group of tumours in this study, mean baseline pO_2 did not provide a good indication of response to hyperoxic gas (ΔpO_2 or pO_{2max}). However, considering the fate of individual voxels in separate tumours with respect to intervention, strong linear correlation was observed in some tumours (tumour #3, 4, 6 and 9) between initial mean baseline pO_2 and the maximum pO_2 at the same location (voxel) in response to carbogen or oxygen breathing consistent with the results of Song *et al* (2002). Other tumours showed no correlation.

The rate of pO_2 response to either gas was similar (figure 6), but decrease upon return to air was significantly faster in the case of oxygen, but not carbogen. While the relationships between ΔpO_2 and $\Delta[HbO_2]$ are not obvious, there exists a significant correlation between f_1/f_2 and mean pO_2 values achieved with hyperoxic gas intervention. Most f_1/f_2 values are between 5 and 60 (figure 7B), implying that the blood perfusion rate in the well perfused region is much higher than that from the poorly perfused region. Not surprisingly the higher the ratio of well-perfused to poorly-perfused regions, the higher the mean pO_2 values achieved by the hyperoxic gas interventions.

Tumor oxygen dynamics by simultaneous NIRS and ^{19}F MRI in rats

Previous studies have demonstrated that tumour tissue oxygenation could be strongly affected by changes in tumour blood flow measured locally by laser Doppler flowmetry (Vaupel *et al* 1994). It was also reported that spontaneous fluctuations in flow and peri-vascular pO_2 are correlated at the on micro-regional level (Kimura *et al* 1996, Braun *et al* 1999). In our study, we are able to derive the perfusion rate ratios between the well perfused and poorly perfused regions from the haemoglobin concentration responses to the intervention measured by NIRS. We found that there was a significant correlation between $d(pO_2)/dt$ and A_1/τ_1 (f_1 proportional to A_1/τ_1), but not $d(pO_2)/dt$ and A_2/τ_2 (f_2 proportional to A_2/τ_2), provided that the pO_2 readings were selected from well oxygenated or responsive voxels (figure 8). This linear correlation suggests that the rate of change in pO_2 is closely related to the perfusion rate in the well perfused region, f_1. In other words, the dynamic changes in pO_2 of those regions responsive to hyperoxic gas intervention may be attributed to fast tumour vascular perfusion, rather than to the slow perfusion in tumour vasculature. We believe these results provide a valuable association between tumour vascular oxygenation and tumour pO_2 determined simultaneously by the optical and NMR measurements.

A goal had been to develop a low-cost, simple, fast surrogate measurement of pO_2 based on NIRS of the oxygenation status of endogenous haemoglobin. Both figures 7B and 8A suggest that there exist linear relationships of pO_2 with the NIRS measurable parameters f_1/f_2 and with A_1/τ_1 that are measurable for NIRS. However, the correlation between ΔpO_2 and $\Delta[HbO_2]$ (figure 7A) seems to be more complex with a separation of the tumours into two groups. It may be noteworthy that the majority (6 of 7) of the tumours associated with the correlation on the left hand side of the graph had a high initial global pO_2 (*i.e.*, mean baseline pO_2 >5 torr), whereas 2 out of 3 of the tumours on the right had low initial global pO_2. A possible interpretation relates to change in the shape of the haemoglobin-oxygen dissociation curve (the Hill curve). A given pO_2 response can correspond to different changes in haemoglobin saturation depending on where the change occurs on the Hill curve. At lower initial pO_2 there may be a substantial ΔpO_2 with little $\Delta[HbO_2]$. By contrast, at higher initial pO_2 the same increase in pO_2 will produce a greater effect on the saturation. While $\Delta[HbO_2]$ is proportional to the change of SO_2 (with the assumption

of little change in total haemoglobin concentration during intervention), two subpopulations of tumours in the relationship between ΔpO_2 and $\Delta[HbO_2]$ could be the result of different initial pO_2. Similarly, two subpopulations of tumours were observed in the relationship between initial SO_2 and the carbogen-induced change in saturation in the study of Hull *et al* (1999). Such an effect also confounds the direct correlation of BOLD MRI response to changes in pO_2 (Baudelet and Gallez 2002). Significantly, preliminary data reported by Gu *et al* (2004a) for simultaneous BOLD MRI and NIR in tumors showed a strong linear correlation in response to hyperoxic gas challenge, as also reported by chen *et al* (2003) in the rat brain.

A major concern is tumour heterogeneity, as recognised throughout the literature and shown here by ^{19}F MRI (figure 4). Indeed, we have obtained some preliminary data using a single NIR source and three detectors placed on various regions across a tumour (Kim *et al* 2003a), showing that each region of the tumour responded differently to hyperoxic gas, in terms of the extent and rate, indicating the heterogeneity of tumour vasculature. Spatial discrimination will be even more critical, if such studies are transferred to human breast cancer, where the tumour is surrounded by normal tissue (Brooksby *et al* 2003). Nevertheless, we believe this haemodynamic model and correlation between tumour vascular oxygenation and pO_2 provides valuable insight into the tumour compartment of such a mixed system and explores dynamic signatures of breast tumours, which could, in turn, enhance/assist human breast cancer diagnosis and prognosis.

In summary, by studying tumour vascular oxygenation concomitantly with changes in tumour oxygen tension, we found several significant correlations between rates and magnitudes of vascular and tissue responses. This study also demonstrates the feasibility of conducting simultaneous NIRS and MRI oximetry. We believe the correlation of tumour vascular oxygenation and tumour tissue pO_2 can provide valuable insights into tumour pathophysiology and response to interventions.

Acknowledgements

This work was supported in part by the Department of Defense Pre-doctoral Research Fellowship W81XWH-04-1-0411 (MX), Breast Cancer Initiative grant DAMD17-00-1-0459 (HL), NIH R01 CA79515/EB002762 (RPM) and Cancer Imaging Program NIH P20 CA086354 (RPM). The MR investigations were performed at the Mary Nell and Ralph B. Rogers NMR Center, a NIH BRTP facility (#P41RR02584). We are grateful to Vincent Bourke and Drs. Anca Constantinescu, Yueqing Gu and Luis Saez for valuable discussions and technical assistance.

Figure Legends

Figure 1

Schematic of experimental set-up. Z is along the bore of the magnet, and X along the axis of the rf coil. PMT represents a photomultiplier tube, I/Q represents an In-phase and Quadrature (I/Q) demodulator chip and ADC represents an analogue to digital converter.

Figure 2

Temporal profiles of $\Delta[HbO_2]$ (curve only) and mean pO_2 (curve with ◆) in response to respiratory challenge. Both $\Delta[HbO_2]$ and pO_2 are group-averaged data from seven 13762NF rat breast tumours with an intervention sequence of air-oxygen-air-carbogen-air, measured simultaneously by NIRS and *FREDOM*. The standard deviations of the volume-averaged baseline pO_2 from 7 tumours are indicated in figure 2. The unit for $\Delta[HbO_2]$ is mM/DPF.

Figure 3

A) Representative dynamic responses of $\Delta[HbO_2]$ to gas intervention (carbogen). The unit for $\Delta[HbO_2]$ is mM/DPF. Single exponential curve fitting yielded $\Delta[HbO_2] = 0.22\{1 - \exp[-(t-106.8)/2.5]\}$ ($R^2=0.64$), and double exponential fitting resulted in $\Delta[HbO_2] = 0.15\{1 - \exp[-(t-106.8)/0.58]\} + 0.13\{1 - \exp[-(t-106.8)/23.2]\}$ ($R^2=0.88$).

B) Relationship of maximum $\Delta[HbO_2]$ (in mM/DPF) in breast tumours in response to switching from air to oxygen and to carbogen ($R^2>0.75$).

Figure 4

Representative pO_2 maps (1.25 mm resolution) obtained using *FREDOM* overlaid on the ^1H anatomic image (FOV= 4 cm x 4 cm). Left) Rat breathing air, Centre) breathing 100% O_2 (fifth map after

switching from air), Right) breathing carbogen (95% O_2 + 5% CO_2) (fifth map after switching from air). The pO_2 maps show distinct heterogeneity.

Figure 5

Correlation between baseline pO_2 and hypoxic fraction (HF_5) measured using *FREDOM* (R^2>0.85).

Figure 6

Mean $d(pO_2)/dt$ (open) and $d(pO_2')/dt$ (shaded) $\pm$ SD for eight tumours with both interventions, when gas was switched from air to the hyperoxic gas and back to air, respectively. pO_2 is the mean value of all acceptable voxels appearing in the five maps during the oxygen or carbogen intervention. $d(pO_2)/dt$ is the slope of regression line of five pO_2 readings versus time during oxygen or carbogen interventions, and $d(pO_2')/dt$ is the slope of regression line for five pO_2 readings versus time during air interventions after oxygen or carbogen. The rates showed a significant difference with oxygen ($p<0.02$), but not with carbogen ($p>0.1$).

Figure 7

A) Correlation between maximum $\Delta[HbO_2]$ and change in pO_2 with respect to hyperoxic gas intervention for two groups of tumours (●) (group 1: #1, 2, 6, 7, 8, 9, 10; $R^2 > 0.51$) and (Δ) (group 2: #3, 4, 5; R^2 >0.82). The unit for $\Delta[HbO_2]$ is mM/DPF.

B) Correlation between mean pO_2 achieved with hyperoxic gas breathing and perfusion rate ratio (f_1/f_2) for tumours with biphasic response to intervention (R^2>0.7). pO_2 is the mean value for the final three pO_2 maps under hyperoxic intervention, selected from all voxels appearing in the final three pO_2 maps during oxygen (◆) or carbogen (□) intervention.

Figure 8

$d(pO_2)/dt$ vs A_1/τ_1 determined from $\Delta[HbO_2]$ for tumours with biphasic response to interventions, showing

a positive correlation (R^2>0.5). pO_2 are obtained from the mean value of all well oxygenated voxels (*i.e.*, the maximum pO_2 > 10 torr under oxygen or carbogen intervention) appearing in the five pO_2 maps during oxygen (◆) or carbogen (□) intervention

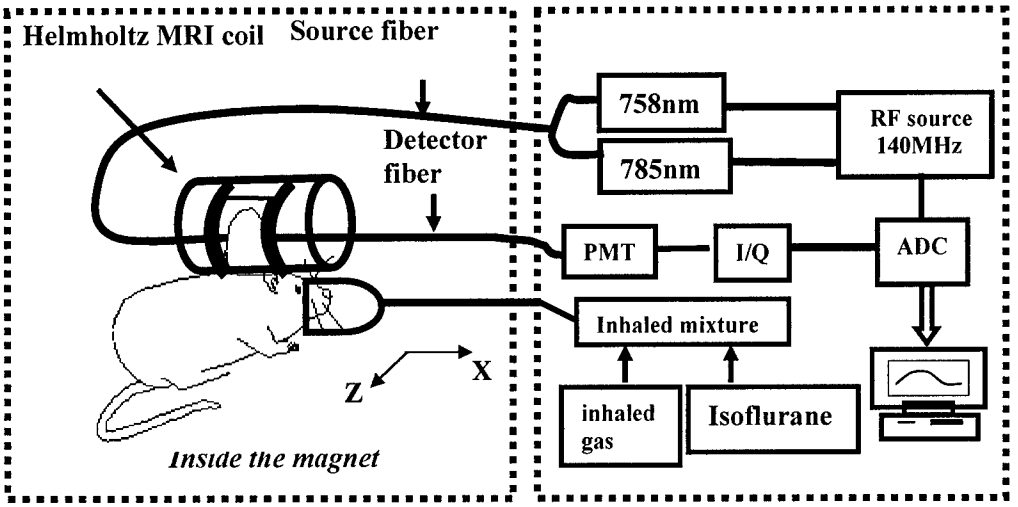
Helmholtz MRI coil
Source fiber
Detector fiber
Z
X
Inside the magnet
758nm
785nm
RF source 140MHz
PMT
I/Q
ADC
Inhaled mixture
inhaled gas
Isoflurane

Figure 1

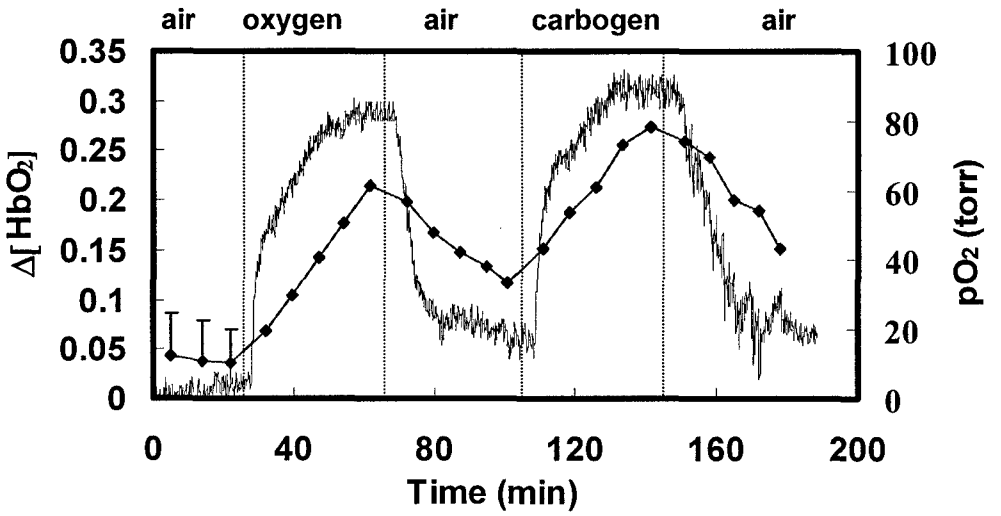
air
oxygen
air
carbogen
air
0.35
0.3
0.25
0.2
0.15
0.1
0.05
0
Δ[HbO2]
100
80
60
40
20
0
pO2 (torr)
0
40
80
120
160
200
Time (min)

Figure 2

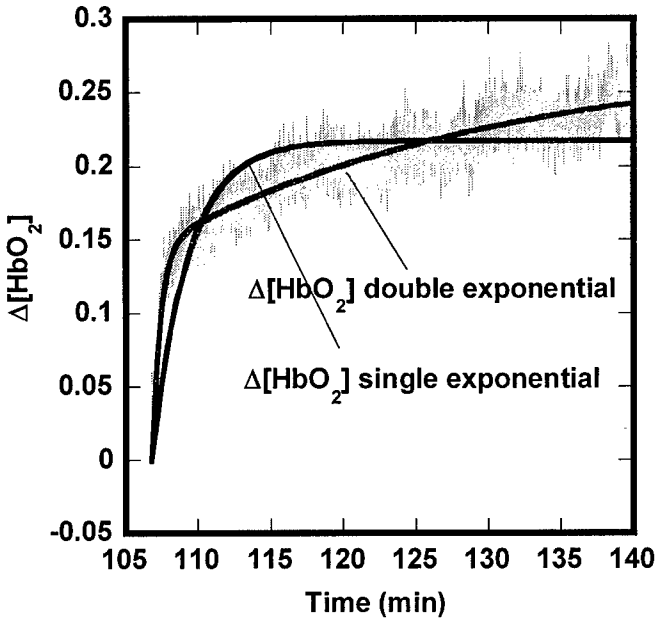

Figure 3A

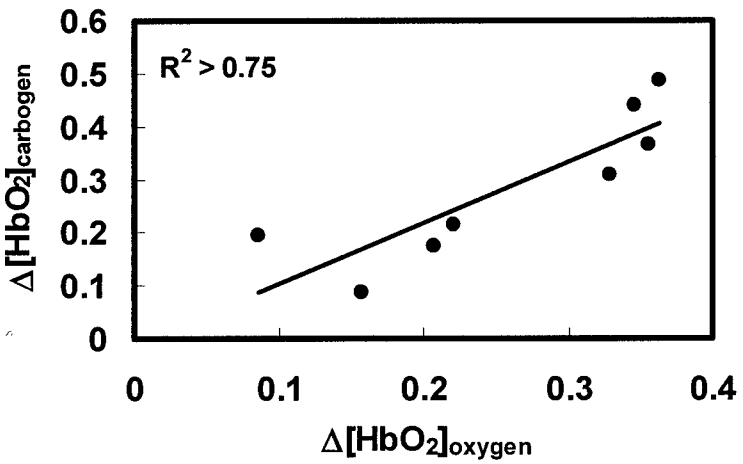

Figure 3B

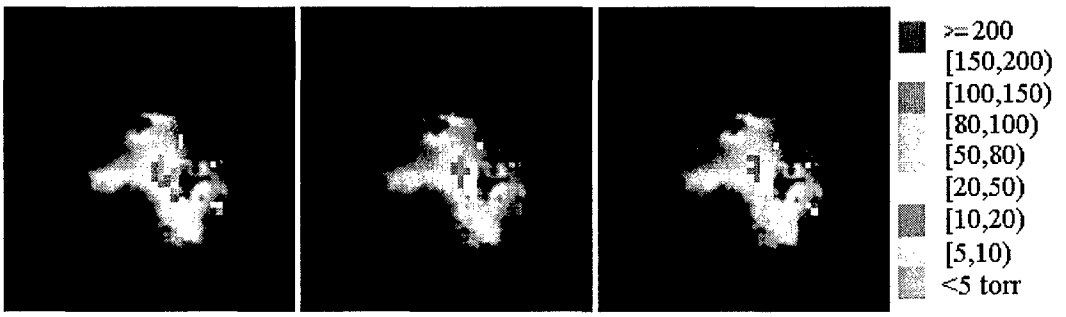

Figure 4

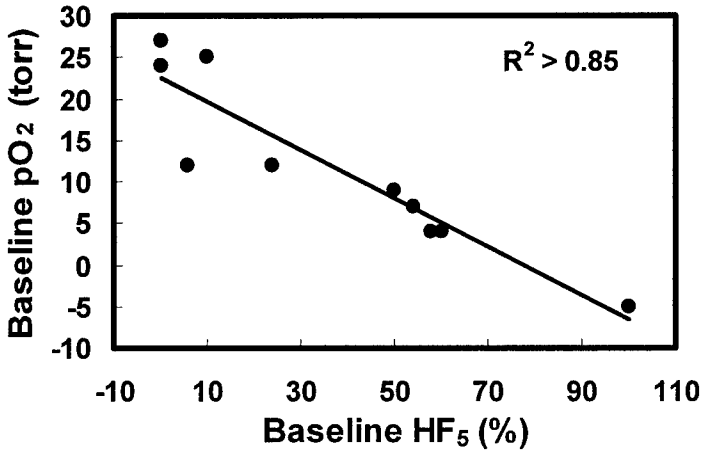
Baseline pO2 (torr)
30
25
20
15
10
5
0
-5
-10
R2 > 0.85
-10
10
30
50
70
90
110
Baseline HF5 (%)

Figure 5

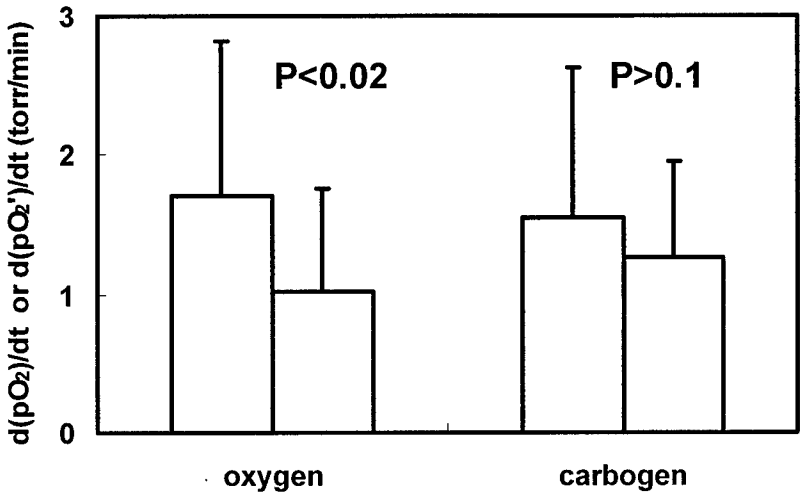

Figure 6

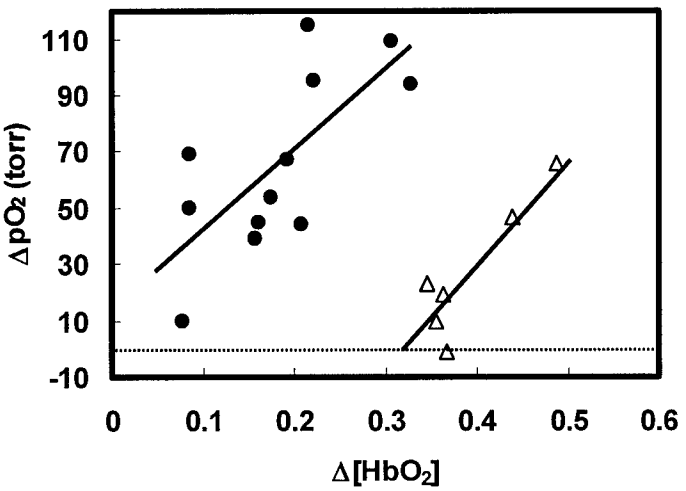

Figure 7A

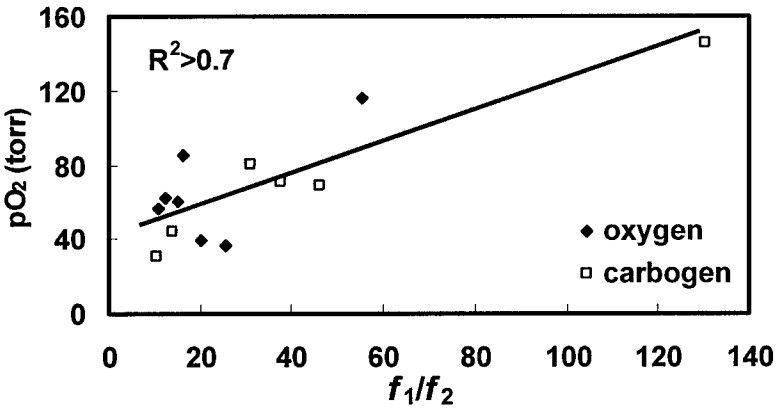

Figure 7B

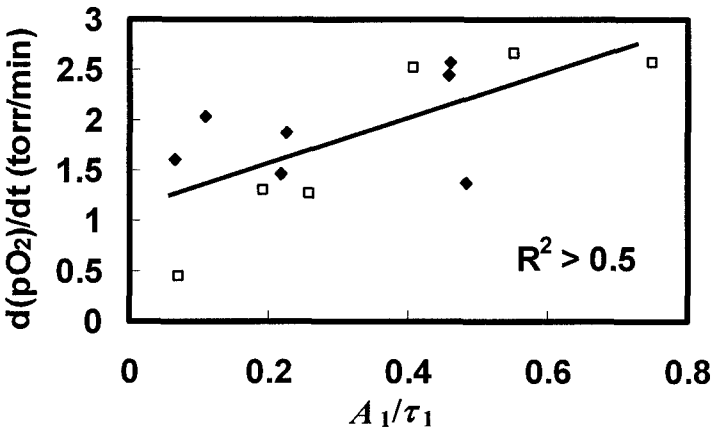

Figure 8

Table 1. Oxygen Tension (pO_2) in ten rat mammary 13762NF adenocarcinomas. pO_2 in baseline is the average value of all voxels in the first three maps, while pO_2 for oxygen or carbogen is the average value of all voxels in the final three pO_2 maps during exposure to the hyperoxic gas. Hypoxic fraction (HF) is the percentage of voxels with pO_2 values less than 5 torr (HF_5) or 10 torr (HF_{10}) and HF_5 and HF_{10} are the average value of final three maps in baseline, oxygen or carbogen respectively. The mean pO_2 increased significantly with both oxygen and carbogen and the value was significantly higher with carbogen. HF_5 was significantly reduced with oxygen or carbogen.

	Tumour		Baseline (air)			Oxygen challenge			Carbogen challenge		
No	Volume (cm^3)	Voxels[a]	pO_2 (Torr) Mean ± SD	HF_5 (%)	HF_{10} (%)	pO_2 (Torr) Mean ± SD	HF_5 (%)	HF_{10} (%)	pO_2 (Torr) Mean ± SD	HF_5 (%)	HF_{10} (%)
1	1.6	26	12 ± 3	24 ± 14	49 ± 15	56 ± 10	22 ± 2	29 ± 8	66 ± 3	0	0
2	0.3	10	12 ± 2	6 ± 12	53 ± 15	62 ± 15	0	0	79 ± 6	0	0
3	0.5	5	4 ± 4	60 ± 20	80 ± 0	14 ± 1	33 ± 12	53 ± 12	3 ± 1	73 ± 12	73 ± 12
4	1.3	14	< 1 torr[b]	100 ± 0	100 ± 0	14 ± 7	19 ± 11	48 ± 30	61 ± 21	0	0
5	0.9	24	24 ± 4	0 ± 0	8 ± 4	47 ± 10	0	0	71 ± 11	0	0
6	1.2	8	4 ± 1	58 ± 7	63 ± 0	43 ± 12	50 ± 22	63 ± 0	73 ± 10	0	0
7	0.8	24	27 ± 2	0 ± 0	3 ± 2	122 ± 21	0	0	142 ± 26	0	0
8	0.6	8	9 ± 6	50 ± 22	63 ± 22	103 ± 26	0	0	118 ± 37	0	0
9	0.7	44	25 ± 1	10 ± 5	26 ± 3	----	--	--	35 ± 3	0	3 ± 3
10	0.7	8	7 ± 6	54 ± 19	75 ± 22	52 ± 18	0	0	----	--	--
Mean ± SD	0.9 ± 0.4	17 ± 12	12 ± 10	36 ± 33	52 ± 31	57 ± 36[c]	14 ± 1[d]	21 ± 27	72 ± 41[b]	8 ± 24[b]	8 ± 24

[a] Number of voxels that provide acceptable data for all 23 pO_2 maps.
[b] $p<0.01$.
[c] $p<0.005$.
[d] $p<0.05$.

Supplementary material

Table 2. Summary of vascular oxygen dynamics for the experimental tumours. Two amplitudes (A_1, A_2) and two time constants (τ_1, τ_2) were determined by curve-fitting the dynamic NIRS measurements using a double-exponential expression. Nine out of 10 tumours were observed to have double-exponential features with either oxygen or carbogen intervention. A_1 is significantly smaller than A_2 with oxygen ($p<0.01$), but no significant differences in carbogen ($p>0.19$).

Tumour		Double exponential fitting				
No.	intervention	A_1 (AU)	A_2 (AU)	τ_1 (min)	τ_2 (min)	R
[a]1	oxygen	0.11 ± 0.002	0.12 ± 0.002	0.49 ± 0.02	6.6 ± 0.2	0.94
	carbogen	0.15 ± 0.001	0.13 ± 0.002	0.58 ± 0.01	23.2 ± 1.1	0.94
[a]2	oxygen	0.03 ± 0.002	0.11 ± 0.005	0.46 ± 0.18	25.6 ± 2.9	0.91
	carbogen	----	----	----	----	----
[a]3	oxygen	0.15 ± 0.001	0.38 ± 0.003	0.31 ± 0.02	20.1 ± 0.39	0.98
	carbogen	0.23 ± 0.005	0.2 ± 0.004	1.2 ± 0.04	10.8 ± 0.45	0.95
[a]4	oxygen	----	----	----	----	----
	carbogen	0.16 ± 0.002	2.3 ± 0.27	0.29 ± 0.02	155.8 ± 21	0.97
[a]5	oxygen	0.12 ± 0.002	0.23 ± 0.002	0.55 ± 0.03	11.6 ± 0.27	0.94
	carbogen	----	----	----	----	----
[a]6	oxygen	0.06 ± 0.001	0.26 ± 0.005	0.13 ± 0.01	31.2 ± 1.1	0.96
	carbogen	0.03 ± 0.001	0.08 ± 0.001	0.04 ± 0.02	13.9 ± 0.6	0.78
[a]7	oxygen	----	----	----	----	----
	carbogen	----	----	----	----	----
[b]8	oxygen	0.11 ± 0.002	0.2 ± 0.001	0.24 ± 0.02	7.1 ± 0.1	0.96
	carbogen	0.2 ± 0.002	0.12 ± 0.001	0.49 ± 0.01	9.1 ± 0.2	0.95
[c]9	carbogen	0.01 ± 0.0004	0.02 ± 0.0004	0.14 ± 0.02	3.9 ± 0.12	0.64
[d]10	oxygen	0.05 ± 0.002	0.03 ± 0.002	0.46 ± 0.05	5.6 ± 0.56	0.68
Mean $\pm$ SD	----	0.11 ± 0.068	0.32 ± 0.59	0.42 ± 0.3	24.9 ± 40.2	----

[a]: air→O_2 →air →carbogen→air.
[b]: air → carbogen → air → O_2 → air.
[c]: air → carbogen → air.
[d]: air → oxygen → air.

References

Arridge S R 1995 Photon measurement density functions: I. Analytical forms *Appl. Opt.* **34** 7395-409

Arridge S R and Schweiger M 1995 Photon measurement density functions: II. Finite element method calculations *Appl. Opt.* **34** 8026-37

Baudelet C and Gallez B 2002 How does blood oxygen level-dependent (BOLD) contrast correlate with oxygen partial pressure (pO2) inside tumors? *Magn Reson Med.* **48** 980-6.

Braun R D, Lanzen J L and Dewhirst M W 1999 Fourier analysis of fluctuations of oxygen tension and blood flow in R3230Ac tumors and muscle in rats *Am. J. Physiol.* **277** H551-68

Brooksby B, Dehghani H, Pogue B and Paulsen K 2003 Near infrared (NIR) tomography breast image reconstruction with a priori structural information from MRI: algorithm development for reconstructing heterogeneities *IEEE J. Select Topics Quantum Electron.* **9** 199-209

Brown J M 1999 The hypoxic cell: a target for selective cancer therapy--eighteenth Bruce F. Cain Memorial Award lecture *Cancer Res.* **59** 5863-70

Chance B 1997 Near infrared images using continuous, phase modulated and pulsed light with quantitation of blood and oxygenation *Ann. New Acad. Sci.* **838** 29-45

Chapman J D, Stobbe C C, Arnfield M R, Santus R, Lee J and McPhee M S 1991 Oxygen dependency of tumor cell killing in vitro by light-activated Photofrin II *Radiat. Res.* **126** 73-9

Chen Y, Tailor D R, Intes X and Chance **B** 2003 Correlation between near-infrared spectroscopy and magnetic resonance imaging of rat brain oxygenation modulation *Phys. Med. Biol.* **48** 417-27

Conover D, Fenton B, Foster T and Hull E 2000 An evaluation of near infrared spectroscopy and cryospectrophotometry estimates of haemoglobin oxygen saturation in a rodent mammary tumour model *Phys. Med. Biol.* **45** 2685-700

Dehghani H, Doyley M, Pogue B, Jiang S, Geng J and Paulsen K 2004 Breast deformation modeling for image reconstruction in near infrared optical tomography. *Phys. Med. Biol.* **49** 1131-45

Delpy D T and Cope M 1997 Quantification in tissue near-infrared spectroscopy *Phil. Trans. R. Soc. Lond. B.* **352** 649-59

Fyles A W, Milosevic M, Wong R, Kavanagh M C, Pintilie M, Sun A, Chapman W, Levin W, Manchul L, Keane T J and Hill R P 1998 Oxygenation predicts radiation response and survival in patients with cervix cancer *Radiother. Oncol.* **48** 149-56

Gu Y, Bourke V A, Kim J G, Constantinescu A, Mason R P and Liu H 2003 Dynamic response of breast tumor oxygenation to hyperoxic respiratory challenge monitored with three oxygen-sensitive parameters *Appl. Opt.* **42** 2960-7

Gu Y, Kodibagkar V, Xia M, Constantinescu A, Mason R and Liu H 2004a Correlation of NIR spectroscopy with BOLD MR imaging of assessing breast tumor vascular oxygen status *Proc. OSA Biomedical Optics Topical Meetings (Miami, FL)*

Gu Y, Mason R P and Liu H 2004b Estimated fraction of tumor vascular blood contents sampled by near infrared spectroscopy and 19F magnetic resonance spectroscopy *Opt. Express* **13** 1724 - 33

Gulsen G, Yu H, Wang J, Nalcioglu O, Merritt S, Bevilacqua F, Durkin A, Cuccia D, Lanning R and Tromberg B 2002 Congruent MRI and near-infrared spectroscopy for functional and structural imaging of tumors *Technol. Cancer Res. Treat.* **1** 497-505

Hahn E W, Peschke P, Mason R P, Babcock E E and Antich P P 1993 Isolated tumor growth in a surgically formed skin pedicle in the rat: a new tumor model for NMR studies *Magn. Reson. Imaging* **11** 1007-17

Hall E J 1994 The oxygen effect and reoxygenation *Radiobiology for the Radiologist* (Philadelphia: J. B. Lippincott)

Hockel M, Schlenger K, Aral B, Mitze M, Schaffer U and Vaupel P 1996 Association between tumor hypoxia and malignant progression in advanced cancer of the uterine cervix *Cancer Res.* **56** 4509-15

Homma S, Fukunaga T and Kagaya A 1996 Influence of adipose tissue thickness on near-infrared spectroscopic signals in the measurement of human muscles *J. Biomed. Opt.* **1** 418-24

Hull E L, Conover D L and Foster T H 1999 Carbogen-induced changes in rat mammary tumour oxygenation reported by near infrared spectroscopy *Br. J. Cancer* **79** 1709-16

Hunjan S, Zhao D, Constantinescu A, Hahn E W, Antich P P and Mason R P 2001 Tumor oximetry: demonstration of an enhanced dynamic mapping procedure using fluorine-19 echo planar magnetic resonance imaging in the Dunning prostate R3327-AT1 rat tumor *Int. J. Radiat. Oncol. Biol. Phys.* **49** 1097-108

Kety S S 1951 The theory and applications of the exchange of inert gas at the lungs and tissues *Pharmacol. Rev.* **3** 1-41

Kim J and Liu H 2005 Investigation of bi-phasic tumor oxygen dynamics induced by hyperoxic gas intervention: a numerical study *Opt. Express* **13** 4465-75

Kim J G, Gu Y, Constantinescu A, Mason R P and Liu H 2003a Non-uniform tumor vascular oxygen dynamics monitored by three-channel near-infrared spectroscopy *Optical Tomography and Spectroscopy of Tissue V*

Kim J G and Liu H 2004 Investigation of breast tumor hemodynamics using tumor vascular phantoms and FEM simulations *Proc. Biomedical Topical Meetings (Miami, FL)*

Kim J G, Zhao D, Song Y, Constantinescu A, Mason R P and Liu H 2003b Interplay of tumor vascular oxygenation and tumor pQ2 observed using near-infrared spectroscopy, an oxygen needle electrode, and 19F MR pO2 mapping *J. Biomed. Opt.* **8** 53-62

Kimura H, Braun R D, Ong E T, Hsu R, Secomb T W, Papahadjopoulos D, Hong K and Dewhirst M W 1996 Fluctuations in red cell flux in tumor microvessels can lead to transient hypoxia and reoxygenation in tumor parenchyma *Cancer Res.* **56** 5522-8

Liu H, Song Y, Worden K L, Jiang X, Constantinescu A and Mason R P 2000 Noninvasive Investigation of Blood Oxygenation Dynamics of Tumors by Near-Infrared Spectroscopy *Appl. Opt.* **39** 5231-43

Mason R P, Hunjan S, Constantinescu A, Song Y, Zhao D, Hahn E W, Antich P P and Peschke P 2003 Tumor oximetry: comparison of 19F MR EPI and electrodes *Adv. Exp. Med. Biol.* **530** 19-27

Mason R P, Ran S and Thorpe P E 2002 Quantitative assessment of tumor oxygen dynamics: molecular imaging for prognostic radiology *J. Cell Biochem.* **39** 45-53

Mazurchuk R, Zhou R, Straubinger R, Chau R and Grossman Z 1999 Functional magnetic resonance (FMRI) imaging of a rat brain tumor model: implications for evaluation of tumor microvasculature and therapeutic response *Magn Reson Imaging* **17** 537-48

Ntziachristos V, Yodh A G, Schnall M and Chance B 2000 Concurrent MRI and diffuse optical tomography of breast after indocyanine green enhancement *Proc. Natl. Acad. Sci. USA* **97** 2767-72

Ntziachristos V, Yodh A G, Schnall M and Chance B 2002 MRI-guided diffuse optical spectroscopy of malignant and benign breast lesions *Neoplasia* **4** 347-54

Overgaard J and Horsman M 1996 Modification of hypoxia-induced radioresistance in tumors by the use of oxygen and sensitizers. *Semin. Radiat. Oncol.* **6** 10-21

Pogue B, Zhu H, Nwaigwe C, McBride T, Osterberg U, Paulsen K and Dunn J 2003 Hemoglobin imaging with hybrid magnetic resonance and near-infrared diffuse tomography *Adv Exp Med Biol* **530** 215-24

Sevick E M, Chance B, Leigh J, Nioka S and Maris M 1991 Quantitation of time- and frequency-resolved optical spectra for the determination of tissue oxygenation *Anal. Biochem.* **195** 330-51

Shah N, Cerussi A, Jakubowski D, Hsiang D, Butler J and Tromberg B 2004 Spatial variations in optical and physiological properties of healthy breast tissue *J. Biomed. Opt.* **9** 534-40

Song Y, Contantinescu A and Mason R 2002 Dynamic breast tumor oximetry: the development of prognostic radiology *Technol. in Cancer Res. & Treatm.* **1** 471-8

Toronov V, Webb A, Choi J, Wolf M, Michalos A, Gratton E and Hueber D 2001 Investigation of human brain hemodynamics by simultaneous near-infrared spectroscopy and functional magnetic resonance imaging *Medical Phys.* **28** 521-7

Vaupel P, Kelleher D K and Engel T 1994 Do changes in tumor blood flow necessarily lead to changes in tissue oxygenation and in bioenergetic status? *Adv. Exp. Med. Biol.* **361** 607-11

Welch M, Halpern H and Kurdziel K 2003 Example of imaging solutions to multi-disease biological challenge--imaging of hypoxia *Acad. Radiol.* **10** 887-90

Yang Y, Liu H, Li X and Chance B 1997 Low-cost frequency-domain photon migration instrument for tissue spectroscopy, oximetry, and imaging *Opt. Eng.* **36** 1562-9

Yodh A G and Boas D A 2003 Functional imaging with diffusing light *Biomedical photonics handbook* ed V Tuan (Florida: CRC)

Zhao D, Constantinescu A, Hahn E W and Mason R P 2001 Tumor oxygen dynamics with respect to growth and respiratory challenge: investigation of the Dunning prostate R3327-HI tumor *Radiat. Res.* **156** 510-20

Zhao D, Constantinescu A, Hahn E W and Mason R P 2002 differential oxygen dynamics in two diverse dunning prostate R3327 rat tumor sublines (MAT-Lu and HI) with respect to growth and respiratory challenge *Int. J. Radiat. Oncol. Biol. Phys.* **53** 744-56

Zhao D, Jiang L and Mason R 2004 Measuring changes in tumor oxygenation *Methods Enzymol.* **386** 378-418